Microstructure and mechanical behavior of 17-4 precipitation hardenable steel processed by selective laser melting

Rafi, H. Khalid; Pal, Deepankar; Patil, Nachiket; Starr, Thomas L.; Stucker, Brent E.

2014

Rafi, H. K., Pal, D., Patil, N., Starr, T. L., & Stucker, B. E. (2014). Microstructure and mechanical behavior of 17-4 precipitation hardenable steel processed by selective laser melting. Journal of materials engineering and performance, 23(12), 4421-4428.

https://hdl.handle.net/10356/103371

https://doi.org/10.1007/s11665-014-1226-y

JMEPEG (2014) 23:4421–4428
DOI: 10.1007/s11665-014-1226-y

1059-9495/$19.00

Microstructure and Mechanical Behavior of 17-4 Precipitation Hardenable Steel Processed by Selective Laser Melting

H.Khalid Rafi, Deepankar Pal, Nachiket Patil, Thomas L. Starr, and Brent E. Stucker

(Submitted April 24, 2014; in revised form July 26, 2014; published online September 12, 2014)

The mechanical behavior and the microstructural evolution of 17-4 precipitation hardenable (PH) stainless steel processed using selective laser melting have been studied. Test coupons were produced from 17-4 PH stainless steel powder in argon and nitrogen atmospheres. Characterization studies were carried out using mechanical testing, optical microscopy, scanning electron microscopy, and x-ray diffraction. The results show that post-process heat treatment is required to obtain typically desired tensile properties. Columnar grains of smaller diameters (<2 μm) emerged within the melt pool with a mixture of martensite and retained austenite phases. It was found that the phase content of the samples is greatly influenced by the powder chemistry, processing environment, and grain diameter.

Keywords austenite-to-martensite phase transformation, microstructure formation, selective laser melting

1. Introduction

Selective laser melting (SLM) has been developed as an additive manufacturing technique for building three-dimensional metallic parts from metal powders, based on the principle of selective laser sintering (SLS) (Ref 1, 2). As compared to SLS, SLM uses a higher power laser source with a wavelength suitable for melting metallic powders (Ref 3). SLM is gaining considerable interest as an advanced manufacturing technique to produce versatile components ranging from biomedical to aerospace applications. In SLM, a planar layer of powdered metallic material is applied onto a base plate above the build platform and a laser scans, the regions in the powder layer according to the profile defined by the computer aided design (CAD) model. The scanning results in localized melting and solidification of the powder to form a layer of the part. Subsequent layers are built one over the other by lowering the build platform equivalent to the layer thickness, spreading a new layer of powder, and scanning the subsequent cross-section, repeating this process until the part is completed. This enables building of complex internal structures which would not be possible with conventional manufacturing processes.

H. Khalid Rafi, J.B Speed School of Engineering, University of Louisville, Louisville, KY 40292 and Department of Mechanical and Aerospace Engineering, School of Mechanical and Aerospace Engineering, Nanyang Technological University, 50 Nanyang Avenue, Singapore 639798, Singapore; and **Deepankar Pal, Nachiket Patil, Thomas L. Starr,** and **Brent E. Stucker**, J.B Speed School of Engineering, University of Louisville, Louisville, KY 40292. Contact e-mails: khalidrafi@gmail.com and khalidrafi@ntu.edu.sg.

The materials that are commercially available for SLM are limited due to the fact that extensive investigations into appropriate process parameter combinations for each different material are required (Ref 4). Common materials which are currently available for SLM include alloys such as Ti-6Al-4V (Ref 5), AISI 316L (Ref 6), 17-4 PH steel (Ref 7), Inconel 625 (Ref 8), M2 high speed steel (Ref 9), and CoCr alloys (Ref 10). Investigations are underway for the development of new process methodologies to extent the application of SLM to other materials. The rapid heating and cooling of small volume of materials each time in SLM provides the potential to fabricate complex parts from metallic glass (MG) powders, which is otherwise rather complicated with other processing routes such as casting and melt spinning. Fabrication of Fe-based MG scaffolds using SLM was shown by Pauly et al. (Ref 11). Li et al. demonstrated the feasibility of fabrication of marginal Al-based MG using SLM (Ref 12). High melting point materials such as tungsten carbide (Ref 13) and tantalum (Ref 14) were also now processed in SLM using high laser powers and slower scan speeds.

Fabrication of metallic composites from pre-mixed powders using SLM is another area of interest. Fe/SiC nanocomposites were fabricated from mixed powders of microsized SiC and Fe particles using SLM. The fabricated nanocomposite exhibited strengths much higher than pure iron sample due to modification in the matrix microstructure, grain refinement and the dislocation pinning by nanoscaled SiC particles (Ref 15). Metal composite of β titanium with randomly dispersed Mo particles were fabricated from pre-alloyed Ti6Al4V-ELI with 10 wt.% Mo powder. The addition of Mo suppressed the transformation of β phase to α′ martensite during fast cooling and completely retained the β phase (Ref 16).

This study focuses on the evolution of microstructure and properties of 17-4 precipitation hardenable (PH) stainless steel when processed by SLM. PH stainless steels are used in applications where both high strength and resistance to corrosion or oxidation are desired. Chromium imparts corrosion resistance, and strength comes from precipitation of submicron

copper precipitates upon aging at elevated temperatures. They have been used extensively in the aircraft, naval, nuclear, and chemical industries due to their excellent mechanical properties, machinability and formability. Among the PH steels, 17-4 PH steel is the most commonly used (Ref 17). 17-4 PH steel is a martensitic PH steel containing 3 wt.% Cu and is strengthened by precipitation of copper in the martensitic matrix (Ref 18). A wide range of mechanical properties can be achieved by heat treating this alloy between 482 and 621 °C (Ref 19). Details on SLM of 17-4 PH steel are limited in open literature (Ref 7, 20).

Very high cooling rates typical for the SLM process can result in non-equilibrium microstructures for PH steels. The microstructure of SLM processed samples can be significantly affected by factors such as high localized heat inputs, very short interaction times, local heat transfer conditions, and processing conditions like scanning velocity, hatch spacing (the distance between two adjacent scan vectors), and scanning strategy. Therefore, it is necessary to have an understanding of the microstructural development and the corresponding mechanical behavior of SLM PH steel parts. The purpose of this work is to investigate the mechanical performance and the microstructural evolution of 17-4 PH steel processed using SLM.

2. Experimental Procedure

SLM was performed in a commercial EOSINT M270 direct metal laser sintering machine using EOS-provided AISI 17-4 composition stainless steel powder. The average particle size was measured using a Microtrac S3000 particle size analyzer and was found to be 39 μm. The particle size distribution is shown in Fig. 1. Process parameters used for building the parts are given in Table 1.

The build chamber was maintained at a pressure of 35 millibars above atmospheric pressure with a constant supply of inert gas. Cylindrical dog-bone shaped tensile samples with dimensions corresponding to ASTM E8 standard were fabricated.

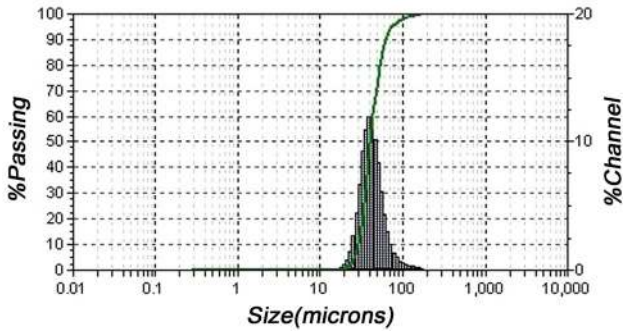

Fig. 1 Powder size distribution for EOS 17-4 PH stainless steel powder

Table 1 Process parameters used to build the samples

Material	Scan speed, mm/s	Power, W	Hatch spacing, mm	Layer thickness, μm
PH steel	800	195	0.10	40

An allowance of 3 mm was given in the diameter for final machining. Samples were built in both nitrogen and argon atmosphere to understand the influence of build environment. A parallel scan strategy with alternating scan direction was adopted and for the successive layers the scanning direction was rotated to 90°. The as-built parts were subjected to different heat treatment steps at 650 °C (for 2 h), 788 °C (for 2 h), and 788 °C (for 2 h) + 482 °C (for 1 h) prior to tensile testing. Tensile specimens were machined from as-built and heat treated specimens according to the dimensions specified by ASTM E8 standard. Tensile testing was performed in an Instron 50 kN test machine (Model: 5569A). A strain rate of 2.5 mm/min was used for the tests.

Microstructural characterization was carried out using optical microscopy (OM), scanning electron microscopy (SEM) and x-ray diffraction (XRD). An Olympus BX53 microscope was used for OM, a high resolution FEG-SEM (FEI NanoSEM) was used to perform electron microscopy and Bruker D8 DISCOVER machine was used for carrying out XRD. Metallographic specimen preparation was carried out following standard procedures. Two different etchants were used to characterize the microstructure. Electrolytic etching with 10% oxalic acid as the electrolyte was used to reveal the austenitic grain boundaries. The electrolytic etching was carried out at 6 V dc for 15 s. Modified Fry's reagent (1 g $CuCl_2$, 25 mL HCl, 25 mL HNO_3, and 150 mL H_2O) was used to reveal the martensitic phase. The microstructural characterization of the samples was carried at the horizontal plane perpendicular to the build direction, herein after referred as plane A, and at the vertical plane parallel to the build direction, herein after referred as plane B. A schematic of the build orientation is shown in Fig. 2.

3. Results

3.1 Tensile Properties

Table 2 shows the tensile results of as-built SLM samples and SLM samples subjected to heat treatment, where the parts were fabricated in a nitrogen environment. Corresponding stress-strain plot is shown in Fig. 3. Among the as-built and the three heat treatment conditions, the as-built sample showed the lowest yield strength. The condition of as-built SLM PH steel samples is similar to that of solution treated PH steel, which was expected to

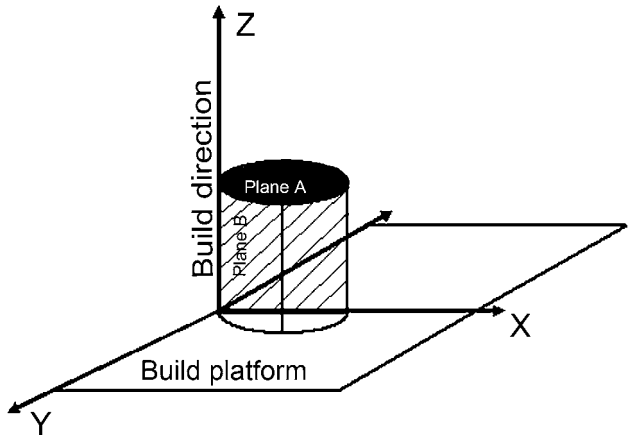

Fig. 2 Schematic representation of the build orientation and the planes at which the microstructural characterization was carried out

result in a higher strength due to the presence of the hard martensitic phase (Ref 21). The lower strength suggests that the as-built SLM PH steel samples are not completely martensitic. A stress relieving heat treatment at 650 °C for 2 h also did not cause much change in the yield strength. However, the heat treatments carried out at 788 °C for 2 h, and 788 °C for 2 h + 482 °C for 1 h resulted in significant change in the tensile strength. The hardening mechanism in PH stainless steel is due to the solid state transformation occurring while heat treating at 788 °C and the precipitation-hardening occurring while aging at 482 °C (Ref 22). However, the tensile strengths obtained for specimens heat treated at 788 °C (solutionised) and 788 + 482 °C (solutionised and aged) are almost similar which means no hardening has occurred during aging. It was also reported by EOS (the SLM machine manufacturer from their in-house experiments) that when the as-built EOS 17-4 PH steel parts were subjected to direct aging at 482 °C the parts did not age harden. They attributed this to the dual phase microstructure observed in the as-built part (both martensitic and austenitic phases) (Ref 23). It is known that the tensile strength of heat treated 17-4 PH steel is a function of the submicron coherent copper precipitates precipitated out from the supersaturated martensitic matrix along the lath boundaries. But the precipitation kinetics becomes sluggish when the austenitic phase co-exists with the martensitic phase. This is because of the higher solubility of copper in the austenitic phase.

It is to be noted that the elongation at break for as-built tested samples is remarkably high when compared to other conditions. Facchini et al. (Ref 7) and Starr et al. (Ref 24) also observed similar behavior. This is because of strain hardening due to the strain induced transformation of retained austenite to martensite. These results suggest the presence of significant amounts of retained austenite along with the martensitic phase. The phases present were thus analyzed by microstructure and XRD, as described below.

3.2 Microstructure

Figure 4 is an optical micrograph from the plane B (parallel to the build direction) of an SLM as-built 17-4 PH stainless steel sample. Melt pool boundaries are distinctly visible, which is in contrast with the microstructure of SLM processed Ti-6Al-4V where the melt pool boundaries are not visible (Ref 25). The average depth of a melt pool is about 60 μm, even though the average powder layer thickness is 40 μm. This is attributed to the higher energy density of the laser beam and the low powder-bed density which is typically about 58%, as observed from in-house experiments. Due to the higher energy input, the top surface of the previously solidified layer is re-melted and forms part of the new melt pool. The vertical separation of two overlapping melt pools can be estimated as the layer thickness. The separation between the melt pool boundaries may vary at different locations due to localized inhomogeneity within the melt pool.

A better understanding of the grain morphology within a solidified melt pool track can be obtained from high magnification SEM-secondary electron (SE) images. Figure 5 shows

Table 2 PH stainless steel tensile properties processed by SLM

Material	Condition	Yield stress, MPa	Ultimate tensile stress, MPa	Elongation at break, %
PH steel	As-built	570 (13)	944 (35)	50 (1)
	650 °C (2 h)	619 (1)	915 (38)	12 (1)
	788 °C (2 h)	857 (14)	1487 (10)	7 (1)
	788 + 482 °C (2 + 1 h)	1126 (14)	1457 (3)	12 (3)
ASM handbook 17-4 PH	482 °C	1170	1310	10

Values in brackets represent standard deviation for three replicates

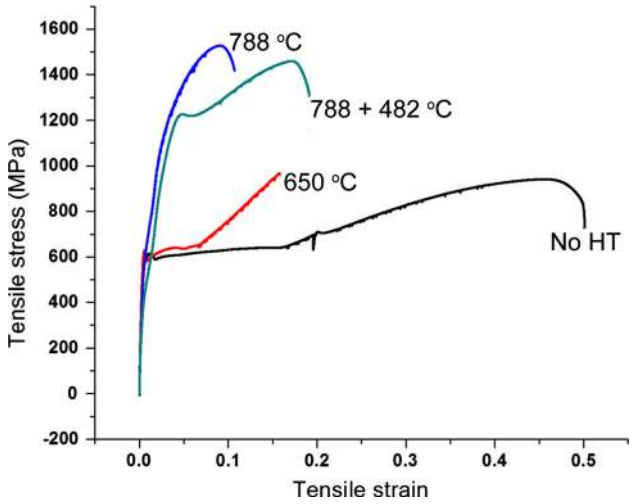

Fig. 3 Stress-strain curves of 17-4 PH stainless steel processed in SLM under N_2 atmosphere for different heat treatment conditions

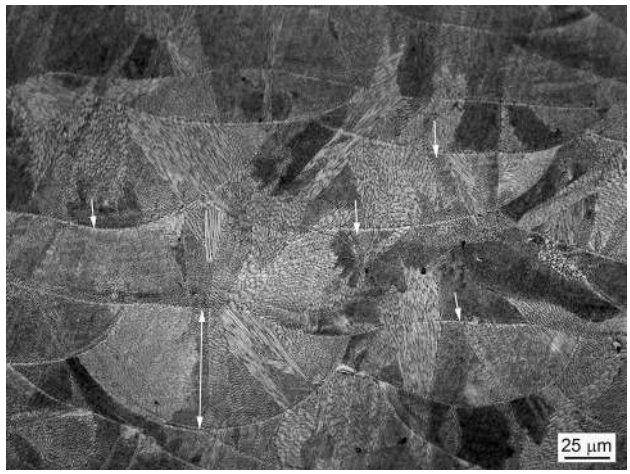

Fig. 4 Optical image of longitudinal cross-section (plane B) of SLM PH steel sample processed in N_2 atmosphere showing distinct melt pools. Short arrow indicates the melt pool boundaries and the line with double arrow head shows the depth of the melt pool

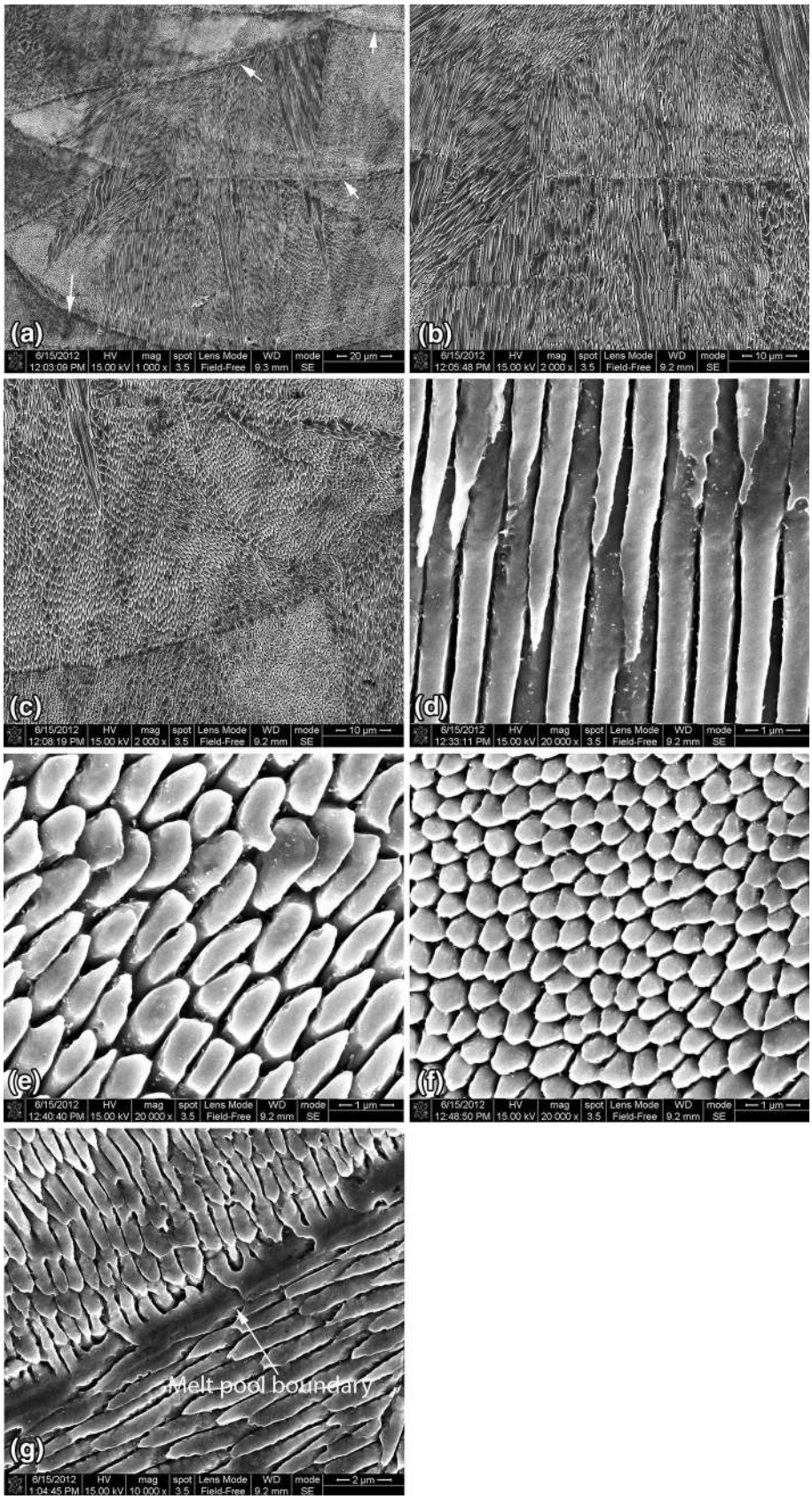

Fig. 5 SEM-SE images of a longitudinal cross-section of a SLM processed 17-4 PH stainless steel part in N_2 atmosphere. (a) Overall view of the melt pool (arrows indicate melt pool boundaries). (b) Magnified image of the left side of a. (c) Magnified image of the right side of a. (d) Columnar grains parallel to the build direction. (e) Columnar grains inclined along the build direction. (f) Columnar grains perpendicular to the build direction. (g) Melt pool boundary

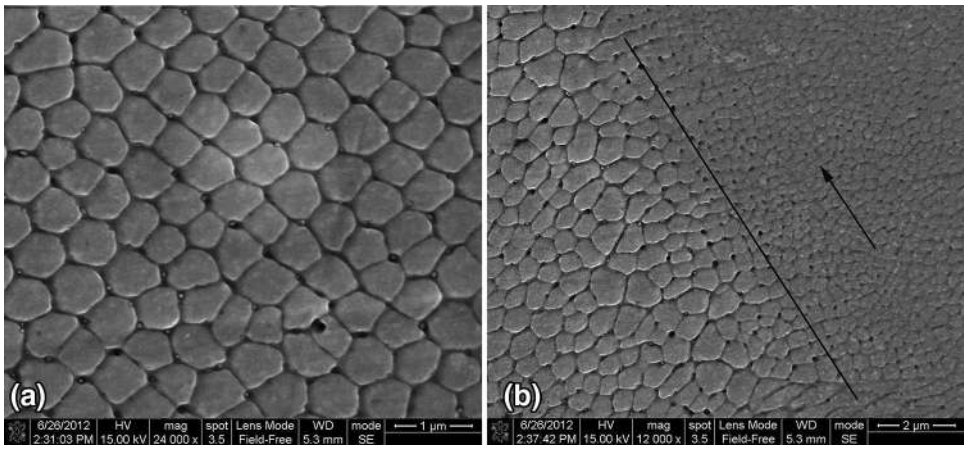

Fig. 6 SEM-SE image of a transverse cross section. (a) Columnar grains with very fine grain diameter. (b) Microstructural difference in adjacent tracks (arrow indicates beam scan direction)

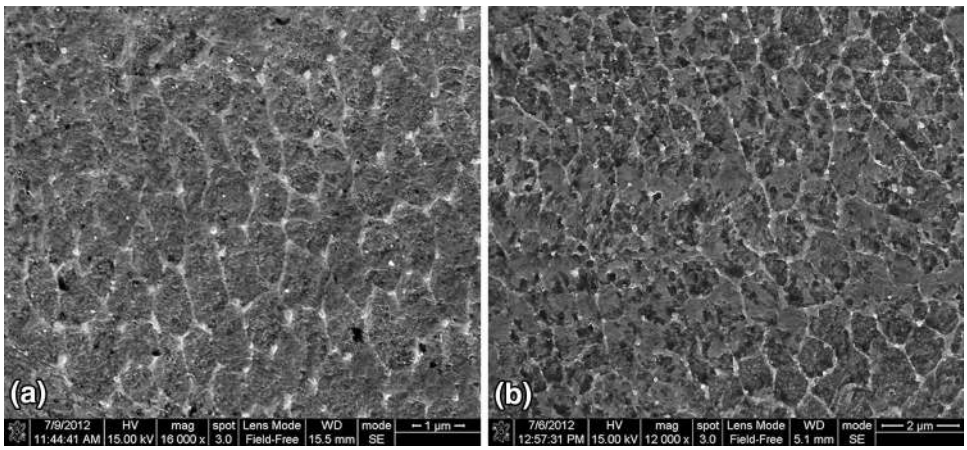

Fig. 7 High magnification SEM-SE images in the transverse cross-section (plane A) of SLM processed 17-4 PH steel sample etched with modified Fry's reagent. (a) Processed in Ar atmosphere, (b) processed in N_2 atmosphere

the SEM-SE image of a region from plane B. An overall view of two overlapping melt pools can be seen in Fig. 5(a). Figure 5(b) and (c) shows magnified image of the left and right side of Fig. 5(a), respectively. The melt pool is characterized by columnar grains oriented in different directions and a few bundles of columnar grains cutting across the melt pool boundaries in the build direction. The microstructural result implies that the direction of dendritic growth is parallel to the heat flow and has a high orientation tendency in the melt pool. Figure 5(d)-(f) shows high magnification images of columnar grains which fall in the longitudinal cutting plane. The columnar grains are parallel (Fig. 5d), inclined (Fig. 5e), or perpendicular (Fig. 5f) to the longitudinal cutting plane. This indicates that the columnar grains grow from multiple locations in the melt pool boundary and grow toward the center of the melt pool. Columnar grains have fine-scale grain diameters, although the length of these grains runs through several layers. It is known that metal parts produced by laser-based methods have finer grain sizes than cast or wrought produced parts. This is due to rapid solidification of the melt pool with cooling rate close to 10^5 K/s (Ref 26). The refinement in grain diameter can be clearly seen in a plane perpendicular to the build direction (plane A in schematic Fig. 2). Figure 6(a) shows the SEM-SE image from the plane A. The grain diameter is found to be less than 1 µm. When the laser beam scans multiple tracks to fill regions within a contour, the previously built track which is adjacent to the melt pool is affected by the thermal excursion. This results in grain coarsening in the adjacent track (Fig. 6b). Even coarsened grains, though, have diameters less than 2 µm.

The microstructural characteristics also showed that the atmosphere used during SLM influences the final microstructure. Figure 7(a) and (b) shows the transverse cross-section (plane A) microstructure of 17-4 PH steels processed under argon atmosphere and nitrogen atmosphere, respectively. The 17-4 PH steel processed under argon atmosphere was comprised of predominantly a martensitic microstructure with some retained austenite whereas the 17-4 PH steel processed under nitrogen atmosphere resulted in a mixture of martensite and retained austenite. The primary reason for retained austenite could be due to the austenite stabilizing effect of nitrogen (Ref 27). In addition to nitrogen purging during the SLM process, another source of nitrogen could be from the powder manufacturing process. The powder supplied by EOS is nitrogen gas atomized. Hence entrapment of nitrogen can be expected in these powders. Chemical analysis of the EOS powder showed the nitrogen content as 0.15%, which is

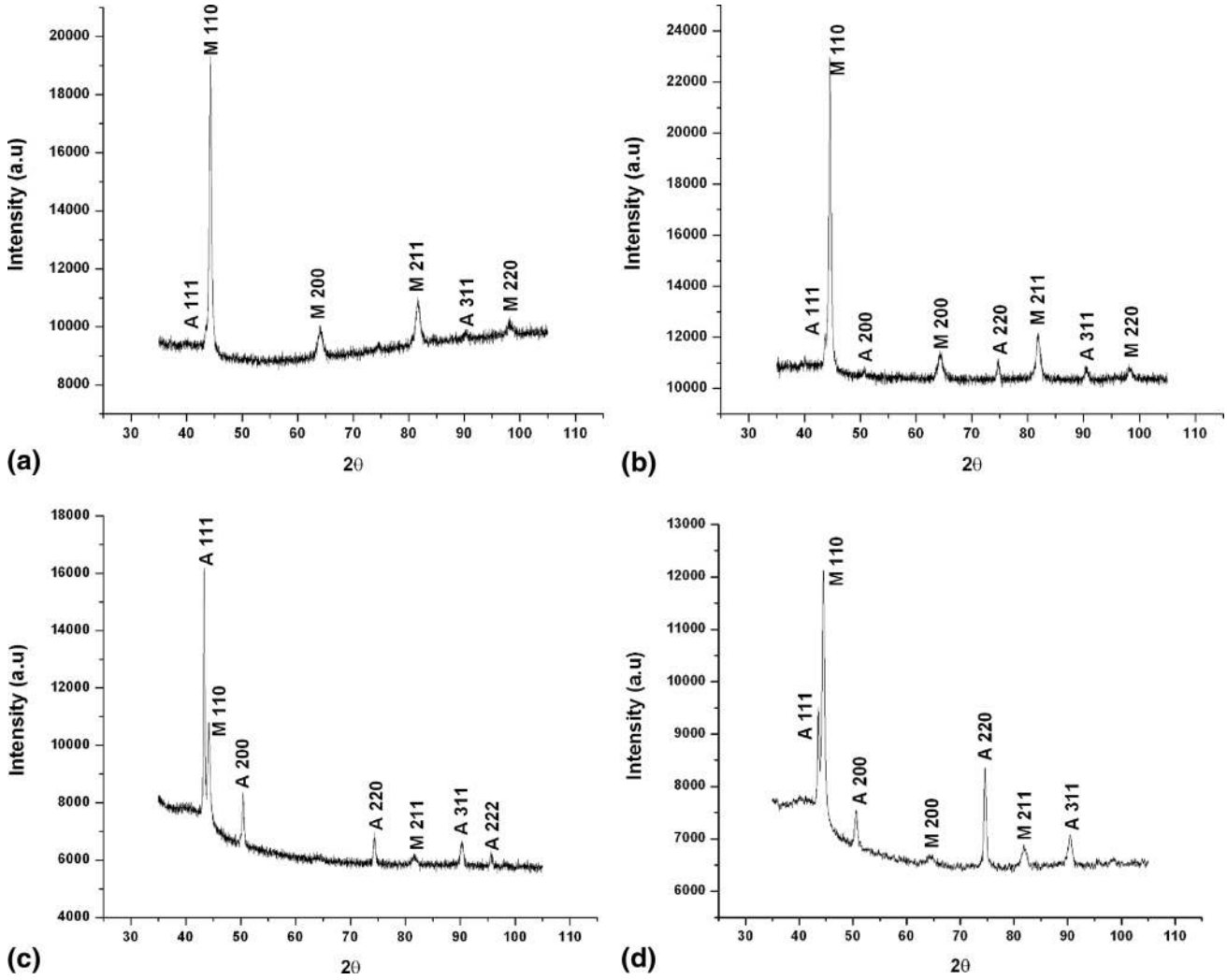

Fig. 8 XRD patterns from 17-4 PH samples: (a) processed in argon atmosphere-longitudinal cross section (plane B), (b) processed in Ar atmosphere-transverse cross section (plane A), (c) processed in nitrogen atmosphere-longitudinal cross section (plane B), (d) processed in nitrogen atmosphere-transverse cross section (plane A)

significant enough to alter the phase composition. Further investigation on the phase compositions were carried out by XRD.

3.3 Phase Analysis

The phase analysis carried out by XRD confirmed the presence of both martensitic and austenitic phases in SLM processed 17-4 PH steels (Fig. 8). The XRD patterns for PH steel processed under argon atmosphere (Fig. 8a and b) shows peaks corresponding to the martensitic phase and very low intensity γ peaks indicating retained austenite. The retained austenitic content was estimated to be about 8%. For PH steel processed under a nitrogen atmosphere (Fig. 8c and d), the γ peak intensities are closer to the peak intensities of the martensitic phase. The percentage of austenitic phase was estimated to about 75% in the vertical plane (plane B) and 50% in the horizontal plane (plane A). Co-existence of both martensitic and austenitic phases in the parts produced in nitrogen atmosphere clearly indicates that the nitrogen atmosphere has influenced the stabilization of austenite. The difference in austenitic and martensitic peak intensities between the horizontal and vertical planes shows the existence of strong texture due to columnar grain formation. The influence of grain alignment with respect to the vertical and horizontal directions is clearly visible for the parts fabricated under N_2 atmosphere (Fig. 8c and d). In the plane parallel (plane B) to the build direction, austenitic peaks showed higher intensity, whereas in the plane perpendicular (plane A) to the build direction martensitic peaks are dominant. This illustrates directionality in crystallographic orientation (texture) associated with the heat transfer conditions in the melt pool, which is also evident from the melt pool microstructure.

4. Discussion

The condition at which the powder is prepared, nitrogen gas atomized or argon gas atomized, and the environment within the build chamber, nitrogen purged or argon purged, influence the final properties of the PH stainless steel parts produced in SLM. In this study, the influence of build environment is mainly addressed. The PH stainless steel powder used was

produced by nitrogen gas atomization by the powder manufacturer. The volume fraction of martensitic phase and austenitic phase in the PH stainless steel parts varied significantly when processed under argon and nitrogen atmospheres. A fully martensitic structure is generally expected when PH stainless steel undergoes rapid cooling after melting. Almost complete martensitic structure with small amount of retained austenite is obtained for SLM PH stainless steel parts when argon is used as the covering gas. However, when the same PH stainless steel powder is processed with nitrogen as the covering gas the microstructure obtained is a mixture of martensitic and retained austenitic phases. This clearly shows the influence of nitrogen on the observed microstructure and the importance of build environment in getting desired microstructure.

The presence of retained austenite and its amount has significant influence on the mechanical properties and performance characteristics of martensitic type stainless steels. The presence of retained austenite can either be detrimental or beneficial depending on the intended application. When a part is put into service, the temperature variations or the loading conditions may cause phase changes in retained austenite, resulting in significant volume changes that lead to cracking (Ref 28). Retained austenite can cause premature wear on sliding and rolling components because it is a softer constitution of the matrix. However, earlier studies have demonstrated the beneficial effects of retained austenite. The studies indicate that the transformation of retained austenite during work hardening allows more plastic strain to be accommodated prior to crack initiation and prevent the propagation of fatigue cracks (Ref 29). Though the presence of retained austenite can provide good toughness, it will severely affect the tensile properties. The retained austenite is a metastable phase which is very sensitive to tensile stresses and hence it could easily transform to fresh and brittle martensite (Ref 30).

Conventionally, cast or wrought 17-4 PH steels are hardened by solutionizing followed by quenching and precipitation hardening. The austenite formed during solutionizing transforms to martensite while quenching through the M_s temperature. The M_s temperature for 17-4 PH steel is typically 132 °C, and the M_f temperature for 17-4 PH steel is typically 32 °C (Ref 31). In a solution annealed condition, very small amount of austenite is retained along the prior austenitic grain boundaries. The strain developed at the high angle boundaries during quenching of the material suppresses the transformation of austenite into martensite in localized regions leading to small amount of austenite being retained in the material (Ref 32). However, a significant amount of austenite will be retained when the M_s and M_f temperature is lowered. The M_s and M_f temperature is influenced by various factors such as the composition of alloying elements, supersaturation of the austenitic phase, residual stress, dislocation density, interdendritic spacing, and grain diameter. Any of these factors can bring down the M_s temperature to room temperature or below. This results in the incomplete transformation of martensite, leading to the retention of significant amount of austenite in the final microstructure. The retained austenite levels increase linearly with decreasing M_s temperature (Ref 28). Also, the stability of retained austenite, which is crucial to the mechanical properties of the steel, is affected by the chemical composition of retained austenite, the size/morphology of retained austenite and the neighboring microconstituents (Ref 33). In SLM, the cooling rates are high enough to form a complete martensitic structure. But the aforementioned factors could influence the volume fraction of retained austenite. As observed from the results, influence of nitrogen is the primary cause for retention of austenite in this case. Along with nitrogen, another factor which might influence the stabilization of austenite could be the grain diameter. The grain diameter of the parent phase has a great effect on the M_s temperature. Takaki et al. (Ref 34) reported that grain refinement of austenite to 1 μm or less is very effective for suppressing the martensitic transformation. The mechanism of austenite stabilization by grain refinement is due to the relationship between austenite grain size and the elastic strain energy required for martensitic transformation. For the martensitic transformation to occur, plastic deformation must be initiated. The shear stress required for the formation of martensite increases with decreasing grain size via the Hall-Petch relationship. This brings down the M_s temperature to room temperature or below. Jiang et al. (Ref 35) proposed a semi-empirical relationship between grain diameter and M_s temperature. Colaco and Vilar (Ref 36) studied this relationship when laser surface melting martensitic stainless steel AISI 420. They found that the M_s decreases slowly from 115 to 100 °C as the grain size changes from 1000 to 50 μm. For grain sizes smaller than 10 μm, the M_s falls sharply, reaching 20 °C when the grain size is 2.7 μm. Another study on surface modification of AISI 420 martensitic type stainless steel using laser engineered near net shaping (LENS) also showed the refinement of austenitic dendrites as the reason for an increase in the amount of retained austenite (Ref 37). In SLM samples, the grain diameter is found to be less than 2 μm. This implies that the finer grain size exhibited by the SLM PH steel samples could also contribute to the degree of retained austenite. Therefore, it can be concluded that the metastable austenite observed in SLM 17-4 PH steel samples are due to the combined effect of nitrogen and the grain refinement.

The amount of retained austenite in SLM 17-4 PH steel samples can be controlled either in-process or by subjecting the part for post-processing. In laser surface melting of tool steels, it was shown that by modifying the laser processing parameters the microstructure can change from almost completely austenitic to almost completely martensitic (Ref 38). Similar approach can be employed in SLM to reduce the retained austenite content by proper combination of laser parameters such as laser power and laser scan speed. The post-processing methods to transform retained austenite to martensite include sub-zero treatment or cryogenic treatment and tempering. Das et al. showed that retained austenite content in a finished tool steel part can be almost completely eliminated by both shallow and deep cryogenic treatments (Ref 39). Tempering is another method to transform retained austenite. Multiple tempers are often performed to ensure the maximum transformation of retained austenite. PH steel processed in SLM can be subjected to above-mentioned methods to transform the retained austenite to ensure the desired microstructure and properties.

5. Conclusions

The mechanical and microstructural features of 17-4 PH steel processed using SLM have been investigated and the results are as follows:

1. The as-built parts have lower yield and ultimate tensile strength as compared to solutionized and aged samples.

2. Elongated columnar grains formed within the melt-pool and few bundles of columnar grains cut across multiple melt-pool boundaries. The orientation of the grains depends on the local heat transfer conditions.
3. The microstructure is comprised of martensite and retained austenite. Parts build under nitrogen atmosphere contains a mixture of both retained austenite and martensite, whereas parts build under argon atmosphere is mostly martensitic with small amount of retained austenite.
4. Stabilization of austenite is enhanced by the presence of nitrogen and the M_s temperature is lowered due to the presence of fine grains that are the result of rapid cooling.

Acknowledgments

The authors thank Office of Naval Research for support through Grant Numbers N00014-09-1-0147 and N00014-10-1-0800.

References

1. F. Abe, K. Osakada, M. Shiomi, K. Uematsu, and M. Matsumoto, The Manufacturing of Hard Tools from Metallic Powders by Selective Laser Melting, *J. Mater. Process. Technol.*, 2001, **111**, p 210–213
2. G.N. Levy, The Role and Future of the Laser Technology in Additive Manufacturing Environment, *Phys. Procedia*, 2010, **5**, p 65–80
3. M. Shellabear and O. Nyrhilä, *DMLS—Development History and State of the Art, LANE 2004 Conference*, Erlangen, Germany, Sept. 21-24, 2004
4. M.S. Wong, C.J. Tsopanos, and I. Sutcliffe, Owen, Selective Laser Melting of Heat Transfer Devices, *Rapid Prototyping J.*, 2007, **13**(5), p 291–297
5. L.E. Murr, S.A. Quinones, S.M. Gaytan, M.I. Lopez, A. Rodela, E.Y. Martinez, D.H. Hernandez, E. Martinez, F. Medina, and R.B. Wicker, Microstructure and Mechanical Behavior of Ti–6Al–4V Produced by Rapid-Layer Manufacturing, for Biomedical Applications, *J Mech. Behav. Biomed.*, 2009, **2**, p 20–32
6. R. Li, Y. Shi, Z. Wang, L. Wang, J. Liu, and W. Jiang, Densification Behavior of Gas and Water Atomized 316L Stainless Steel Powder During Selective Laser Melting, *Appl. Surf. Sci.*, 2010, **256**(13), p 4350–4356
7. L. Facchini, N. Vicente, Jr., I. Lonardelli, E. Magalini, P. Robotti, and A. Molinari, Metastable Austenite in 17–4 Precipitation-Hardening Stainless Steel Produced by Selective Laser Melting, *Adv. Eng. Mater.*, 2010, **12**(3), p 184–189
8. C.P. Paul, P. Ganesh, S.K. Mishra, P. Bhargava, J. Negi, and A.K. Nath, Investigating Laser Rapid Manufacturing for Inconel-625 Components, *Opt. Laser Technol.*, 2007, **39**, p 800–805
9. Z.H. Liu, D.Q. Zhang, and C.K. Chua, Crystal Structure Analysis of M2 High Speed Steel Parts Produced by Selective Laser Melting, *Mater. Charact.*, 2013, **84**, p 72–80
10. A. Takaichi, T. Nakamoto, N. Joko, N. Nomura, Y. Tsutsumi, and S. Migita, Microstructure and Mechanical Properties of Co-29Cr-6Mo Alloy Fabricated by Selective Laser Melting Process for Dental Applications, *J. Mech. Behav. Biomed. Mater.*, 2013, **21**, p 67–76
11. S. Pauly, L. Loeber, R. Petters, M. Stoica, S. Scudino, U. Kuehn, and J. Eckert, Processing Metallic Glasses by Selective Laser Melting, *Mater. Today*, 2013, **16**, p 37–41
12. X.P. Li, C.W. Kang, H. Huang, L.C. Zhang, and T.B. Sercombe, Selective Laser Melting of an $Al_{86}Ni_6Y_{4.5}Co_2La_{1.5}$ Metallic Glass: Processing, Microstructure Evolution and Mechanical Properties, *Mater. Sci. Eng., A*, 2014, **606**, p 370–379
13. D. Gu and Q. Jia, Novel Crystal Growth of In Situ WC in Selective Laser Melted W-C-Ni Ternary System, *J. Am. Ceram. Soc.*, 2014, **97**(3), p 684–687
14. L. Thijs, M.L.M. Sistiaga, R. Wauthle, Q. Xie, J.P. Kruth, and J.V. Humbeeck, Strong Morphological and Crystallographic Texture and Resulting Yield Strength in Selective Melted Tantalum, *Acta Mater.*, 2013, **61**(12), p 4657–4668
15. B. Song, S. Dong, and C. Coddet, Rapid In Situ Fabrication of Fe/SiC Nanocomposites by Selective Laser Melting Directly from a Mixed Powder of Microsized Fe and SiC, *Scripta Mater.*, 2014, **75**, p 90–93
16. B. Vrancken, L. Thijis, J.P. Kruth, and J.V. Humbeeck, Microstructure and Mechanical Properties of a Novel β Titanium Metallic Composite by Selective Laser Melting, *Acta Mater.*, 2014, **68**, p 150–158
17. W.F. Smith, *Structure and Properties of Engineering Alloys*, 2nd ed., McGraw-Hill Inc., New York, 1993, p 328–335
18. M. Murayama, Y. Katayama, and K. Hono, Microstructural Evolution in a 17-4 PH Stainless Steel after Aging at 400°C, *Metall. Mater. Trans. A*, 1999, **30A**, p 345–353
19. K.C. Hsu and C.K. Lin, High-Temperature Fatigue Crack Growth Behavior of 17-4 PH Stainless Steels, *Metall. Mater. Trans. A*, 2004, **35A**, p 3018–3024
20. P.G.E. Jerrard, L. Hao, and K.E. Evans, Experimentation Investigation into Selective Laser Melting of Austenitic and Martensitic Stainless Steel Powder Mixtures, *J Manuf. Eng.*, 2009, **223**(11), p 1409–1416
21. J.H. Wu and C.K. Lin, Tensile and Fatigue Properties of 17-4 PH Stainless Steel at High Temperatures, *Metall. Mater. Trans. A*, 2002, **33A**, p 1715–1724
22. U.K. Viswanathan, S. Banerjee, and R. Krishnan, Effects of Aging on the Microstructure of 17-4 PH Stainless Steel, *Mater. Sci. Eng., A*, 1988, **104**, p 181–189
23. M. Shellabear and O. Nyrhila, *Materials for Direct Metal Laser-Sintering*, White Paper, EOS GmbH
24. T.L. Starr, T.J. Gornet, J.S. Usher, and C. M. Scherzer, "DMLS Mechanical Properties: Tensile and Fatigue Properties of GP1," EOS North America Users Day, May 17, 2010
25. L. Thijs, F. Verhaeghe, T. Craeghs, J.V. Humbeeck, and J.P. Kruth, A Study of the Microstructural Evolution During Selective Laser Melting of Ti-6Al-4V, *Acta Mater.*, 2010, **58**, p 3303–3312
26. T. Vilaro, C. Colin, and J.D. Bartout, As-Fabricated and Heat-Treated Microstructures of the Ti-6Al-4V Alloy Processed by Selective Laser Melting, *Metall. Mater. Trans. A*, 2011, **42**, p 3190–3199
27. E.A. Ul'yanin, N.A. Sorokina, and M. Zaretskii Ya, Properties of Austenitic Steel with Nickel and Nitrogen at Low Temperatures, *Met. Sci. Heat Treat.*, 1969, **11**(9), p 681–682
28. W. Wu, L.Y. Hwu, D.Y. Lin, and J.L. Lee, The Relationship Between Alloying Elements and Retained Austenite in Martensitic Stainless Steel Welds, *Scripta Mater.*, 2000, **42**, p 1071–1076
29. H.J. Kim and Y.G. Kweon, The Effects of Retained Austenite on Dry Sliding Wear Behavior of Carburized Steels, *Wear*, 1996, **193**(1), p 8–15
30. A. Kokosza and J. Pacyna, Evaluation of Retained Austenite Stability in Heat Treated Cold Work Tool Steel, *J. Mater. Process. Technol.*, 2005, **162**, p 327–331
31. A.K. Bhaduri, S. Sujith, G. Srinivasan, T.P.S. Gill, and S.L. Mannan, Optimized Post Weld Heat Treatment Procedures for 17-4 PH Stainless Steels, *Weld. J. Res. Suppl.*, 1995, **51**, p 153–159
32. B. Rajan, S. Roychowdhury, K. Vivekanand, and V.S. Raja, Effect of Reverted Austenite on Mechanical Properties of Precipitation Hardenable 17-4 Stainless Steel, *Mater. Sci. Eng., A*, 2013, **568**, p 127–133
33. S. Zhang and K.O. Findley, Quantitative Assessment of the Effects of Microstructure on the Stability of Retained Austenite in TRIP Steels, *Acta Mater.*, 2013, **61**(6), p 1895–1903
34. S. Takaki, K. Fukunaga, J. Syarif, and T. Tsuchiyama, Effect of Grain Refinement on Thermal Stability of Metastable Austenitic Steel, *Mater. Trans.*, 2004, **45**(7), p 2245–2251
35. B.H. Jiang, L. Sun, R. Li, and T.Y. Hsu, Influence of Austenite Grain Size on γ-ε Martensitic Transformation Temperature in Fe-Mn-Si-Cr Alloys, *Scripta Metall. Mater.*, 1995, **33**(1), p 63–68
36. R. Colaco and R. Vilar, Stabilisation of Retained Austenite in Laser Surface Melted Tool Steels, *Mater. Sci. Eng., A*, 2004, **385**, p 123–127
37. B. Vamsi Krishna and A. Bandyopadhyay, Surface Modification of AISI, 410 Stainless Steel Using Laser Engineered Net Shaping (LENS™), *Mater. Des.*, 2009, **30**, p 1490–1496
38. R. Colaco and R. Vilar, Effect of the Processing Parameters on the Proportion of Retained Austenite in Laser Surface Melted Tool Steels, *J. Mater. Sci. Lett.*, 1998, **17**(7), p 563–567
39. D. Das, A.K. Dutta, and K.K. Ray, Sub-zero Treatments of AISI, D2 steel: Part I. Microstructure and Hardness, *Mater. Sci. Eng., A*, 2010, **527**, p 2182–2193